THE JOURNAL OF PHYSICAL CHEMISTRY A

Article

pubs.acs.org/JPCA

Time-Resolved EPR Study of Singlet Oxygen in the Gas Phase

Marco Ruzzi,[†] Elena Sartori,[‡] Alberto Moscatelli,[‡] Igor V. Khudyakov,*[,‡,§] and Nicholas J. Turro[‡]

[†]Department of Chemical Sciences, University of Padova, 35100 Padova, Italy

[‡]Chemistry Department, Columbia University, New York, New York 10027, United States

ABSTRACT: X-band EPR spectra of singlet $O_2(^1\Delta_g)$ and triplet $O_2(^3\Sigma_g^-)$ were observed in the gas phase under low molecular-oxygen pressures P_{O_2} = 0.175−0.625 Torr, T = 293−323 K. $O_2(^1\Delta_g)$ was produced by quenching of photogenerated triplet sensitizers naphthalene C_8H_{10}, perdeuterated naphthalene, and perfluoronaphthalene in the gas phase. The EPR spectrum of $O_2(^1\Delta_g)$ was also observed under microwave discharge. Integrated intensities and line widths of individual components of the EPR spectrum of $O_2(^3\Sigma_g^-)$ were used as internal standards for estimating the concentration of O_2 species and P_{O_2} in the EPR cavity. Time-resolved (TR) EPR experiments of C_8H_{10} were the main focus of this Article. Pulsed irradiation of C_8H_{10} in the presence of $O_2(^3\Sigma_g^-)$ allowed us to determine the kinetics of formation and decay for each of the four components of the $O_2(^1\Delta_g)$ EPR signal, which lasted for only a few seconds. We found that the kinetics of EPR-component decay fit nicely to a biexponential kinetics law. The TR EPR 2D spectrum of the third component of the $O_2(^1\Delta_g)$ EPR spectrum was examined in experiments using C_8H_{10}. This spectrum vividly presents the time evolution of an EPR component. The largest EPR signal and the longest lifetime of $O_2(^1\Delta_g)$, τ = 0.4 s, were observed at medium pressure P_{O_2} = 0.4 Torr, T = 293 K. The mechanism of $O_2(^1\Delta_g)$ decay in the presence of photosensitizers is discussed. EPR spectra of $O_2(^1\Delta_g)$ evidence that the spin-rotational states of $O_2(^1\Delta_g)$ are populated according to Boltzmann distribution in the studied time range of 10−100 ms. We believe that this is the first report dealing with the dependence of $O_2(^1\Delta_g)$ EPR line width on P_{O_2} and T.

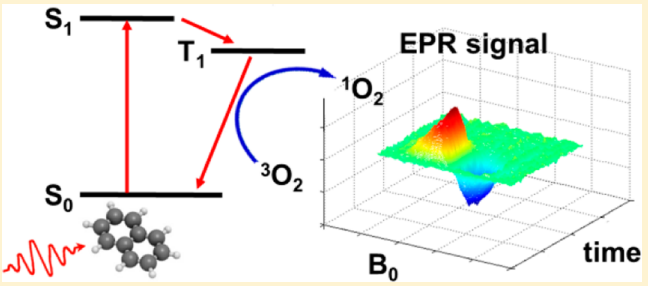

1. INTRODUCTION

Singlet oxygen $O_2(^1\Delta_g)$ is an important intermediate in many photochemical and photobiological processes.[1] The physical and chemical properties of $O_2(^1\Delta_g)$ have been the subject of extensive investigations during the last several decades.[2−7] At least 100 publications, numerous review articles, and many books are devoted to $O_2(^1\Delta_g)$ in the condensed phase. The detection of $O_2(^1\Delta_g)$ and the monitoring of its reactions in solution commonly are accomplished through the observation of the characteristic luminescence of $O_2(^1\Delta_g)$ at 1270 nm.[2−6]

Although $O_2(^1\Delta_g)$ does not possess a net electronic spin, it is paramagnetic because of its net electron orbital angular momentum J = 2 and is therefore expected to possess an electron paramagnetic resonance spectrum (EPR). The EPR spectrum of $O_2(^1\Delta_g)$ has not been reported in liquid solutions. However, there are reports on the EPR spectrum of $O_2(^1\Delta_g)$ in the gas phase.[8−14] To the best of our knowledge, there are fewer than 10 scattered and dated reports on EPR of $O_2(^1\Delta_g)$ under low pressure.[8−14] EPR of $O_2(^1\Delta_g)$ was reported for the first time in 1965.[8] One communication presented data on the kinetics of $O_2(^1\Delta_g)$ formation and decay in the gas phase measured by EPR in which its lifetime was τ = 7 s.[14] The contributions of different decay processes in the determined τ[14] remain unknown.

Because $O_2(^1\Delta_g)$ is one of the pollutants in the atmosphere of large cities, the investigation of the kinetics of formation and decay of $O_2(^1\Delta_g)$ is interesting not only as a subject of gas-phase kinetics and gas-phase EPR but also from an environmental standpoint.[15,16] UV photolysis of ozone in the upper layers of the atmosphere also leads to the formation of $O_2(^1\Delta_g)$.[17]

The reported EPR spectrum of $O_2(^1\Delta_g)$ has four components whose origins are well understood on the basis of rotational spectroscopy.[8,14] Thus, the EPR of $O_2(^1\Delta_g)$ can serve as a convenient fingerprint of this electronically excited molecule in the gas phase.

Two established methods for the gas-phase generation of $O_2(^1\Delta_g)$ are the creation of a microwave discharge in $O_2(^3\Sigma_g^-)$ and the quenching of the triplet states of sensitizers (^{3}Sens*) by $O_2(^3\Sigma_g^-)$, as shown in eq 1:

$$^3\text{Sens}^* + O_2(^3\Sigma_g^-) \rightarrow {}^1\text{Sens} + O_2(^1\Delta_g) \quad (1)$$

Here, we report a time-resolved (TR) EPR kinetic study of $O_2(^1\Delta_g)$ produced in eq 1 under different pressures P_{O_2} and temperatures T. In addition, we demonstrate $O_2(^1\Delta_g)$ generation by microwave discharge to compare EPR spectra of $O_2(^1\Delta_g)$ obtained by the method of eq 1 with that of naphthalene ($C_{10}H_8$) and its derivatives as photosensitizers (Sens).

Received: January 18, 2013
Revised: May 28, 2013
Published: June 3, 2013

   dx.doi.org/10.1021/jp403648d | J. Phys. Chem. A 2013, 117, 5232−5240

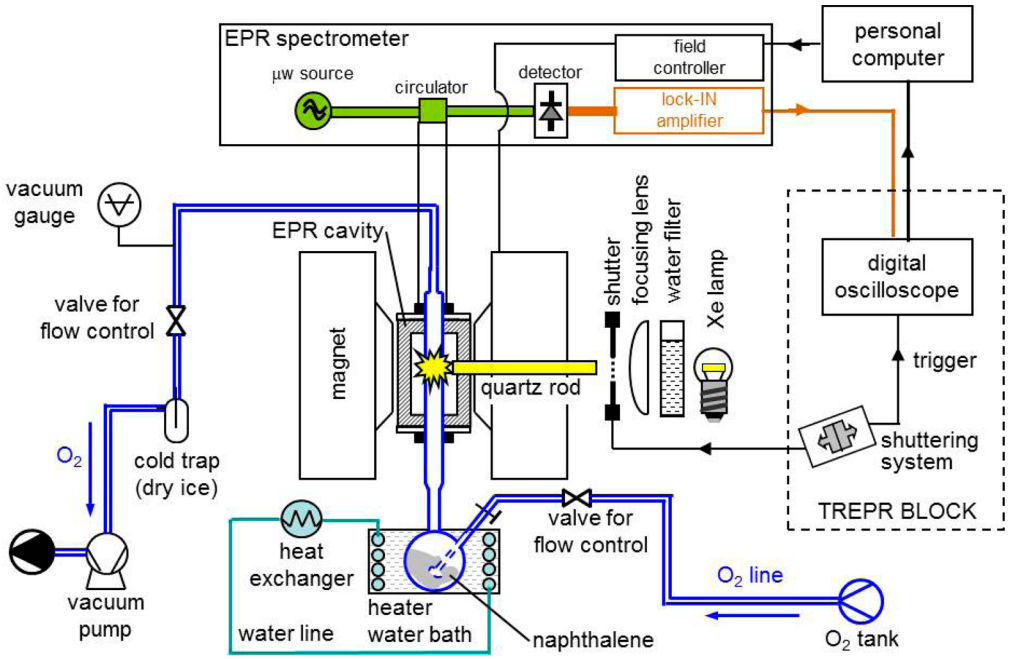

Figure 1. Schematic of the experimental setup for CW EPR and TR EPR detection of gas-phase $O_2(^1\Delta_g)$ generated in continuous and pulsed-light sensitization experiments.

2. EXPERIMENTAL SECTION

2-1. EPR Setup for the Observation of EPR Spectra of Oxygen in the Gas Phase. A Bruker Elexsys X-band EPR spectrometer with a large sample access Bruker gas-phase EPR cavity (model WZ 4107 AC) was employed in this investigation. An EPR cell consisting of either a sealed quartz tube or a flow quartz tube was used. The internal diameter of both cells was 10 mm. In all cases, O_2 in the cell was under low pressure as described below. A conventional 100 kHz field-modulation lock-in system (phase-sensitive detection) was used to detect the EPR signal as a function of both the magnetic field and time. An amplitude modulation of 1 G and a microwave attenuation of 5 dB were used unless stated otherwise. All spectra are presented in a standard manner (i.e., as the first derivative of the signal).

$O_2(^1\Delta_g)$ was produced in the discharge experiments by flowing pure O_2 at P_{O_2} < 1 Torr through a CW microwave-discharge generator (Opthos MPG-4 CW microwave generator equipped with an Evenson tuning cavity). The generator was placed at an experimentally determined optimal distance of 30 cm from the EPR cavity. There was no electric interference with the discharge when using a microwave bridge at this distance, and $O_2(^1\Delta_g)$ was found to be produced in a sufficient concentration downstream in the cavity to produce acceptable EPR signals in spite of the partial decay of $O_2(^1\Delta_g)$ that takes place during its movement through the 30 cm flow cell. The O_2 flow rates were measured by a capillary flow meter and generally were in the range of $(2-5) \times 10^{-7}$ M/s. We estimated the residence time of O_2 in the cavity to be 0.05−1.0 s.

In experiments with Sens, $O_2(^1\Delta_g)$ was produced by mixing Sens with O_2 and passing the gas mixture through the flow cell. The mixing took place in a Pyrex flask that was 9 cm from the EPR cavity (Figure 1).

A flask containing O_2 and $C_{10}H_8$ was completely immersed in a thermostated water bath and kept at T = 293−318 K. The system allows the flow of O_2 from the bottom to the top of the flask with O_2 streaming through 20 g of Sens placed inside the flask, as shown in Figure 1. To avoid the condensation of $C_{10}H_8$ and Sens, a heating-tape system was used to keep the temperature constant over the entire quartz tube between the flask and the cavity. The EPR cavity was thermostated. This setup established a constant temperature in the whole flask−quartz tube−EPR cavity system. Thus, we report the temperatures of the gas inside the cavity of the EPR cell as being equal to the temperatures of Sens in the flask.

The pressure of the flowing gas was measured with a vacuum-gauge controller (Sargent-Welch) located within the vacuum pump (Alcatel 2012A). Because of the controller position, it is likely that the gas-pressure controller readings somewhat underestimated the real P_{O_2} in the EPR cavity. However, the line widths of the EPR components of $O_2(^3\Sigma_g^-)$ (cf. section 3-3) strongly depend on P_{O_2} (i.e., the higher the pressure, the broader the line widths, cf. Results and Discussion). Thus, line widths can be used for measurements of pressure after proper calibration (Figure 2).

We found that line widths of components of the EPR spectrum of $O_2(^3\Sigma_g^-)$ allow for an estimation of P_{O_2} in the cavity with an experimental uncertainty that is smaller than 10%. We used calibration curves to specify the P_{O_2} values presented in this Article. Unless stated otherwise, P_{O_2} is the total pressure of gases in either the sealed or flow cells. Irradiation of Sens in the presence of $O_2(^3\Sigma_g^-)$ or a microwave discharge does not change P_{O_2} because the total concentration of O_2 stays the same and Sens undergoes minor negligible consumption under short irradiation.

The optical excitation of Sens was carried out by employing a continuous UV−vis 300 W Xe lamp filtered by 5 cm of distilled water. A collimating lens (with the addition of an optical quartz rod in some experiments) was used for the irradiation of samples in the EPR cavity (Figure 1). The broad-wavelength emission band of the excitation light overlaps with the absorption maximum (ca. 310 nm) of naphthalene and its derivatives. Samples were irradiated with the light at λ > 220 nm.

dx.doi.org/10.1021/jp403648d | J. Phys. Chem. A 2013, 117, 5232−5240

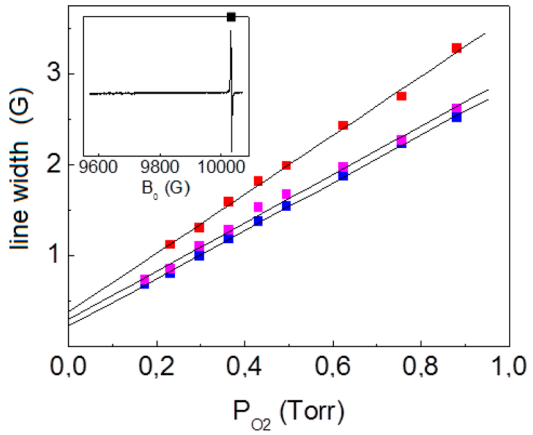

Figure 2. Line widths of a selected $O_2(^3\Sigma_g^-)$ EPR spectrum component as a function of P_{O_2} from flow experiments with pure $O_2(^3\Sigma_g^-)$ (flask without Sens), T = 290 K (blue filled boxes) or with a gas mixture of $O_2(^3\Sigma_g^-)$ and $C_{10}H_8$, T = 290 K (pink filled boxes) and 318 K (red filled boxes).

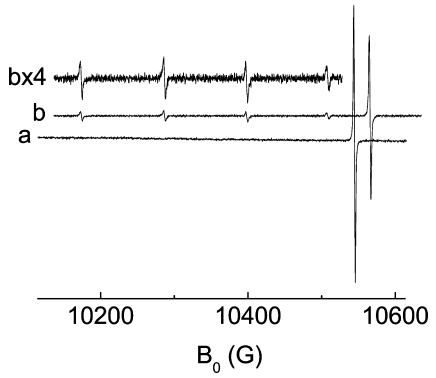

Figure 3. EPR spectra in the sealed cell containing O_2 (P_{O_2}= 0.2 Torr) and $C_{10}H_8$ vapor (estimated $P_{C_{10}H_8}$ = 82 mTorr) obtained in the dark (a) and during irradiation, T = 293 K. The intensity component in the high field (a,b) is part of the EPR of $O_2(^3\Sigma_g^-)$. The EPR spectrum of $O_2(^1\Delta_g)$ consisting of four components (b and bx4) was obtained under photoexcitation. Each spectrum is the result of a single scan with an acquisition time of 167 s.

In the TR-EPR experiments (see the TR-EPR block in Figure 1), we used an electromechanical shutter (UniBlitz, model D122 Shutter Driver) controlled by a pulse generator (Stanford Research Systems, model DG535). Light-irradiation periods were 1.5 s, and dark, 3.5 s, with a shutter frequency of 0.2 Hz. A pulse generator triggered the acquisition of EPR spectra.

The time resolution of the EPR measurements is dependent upon the time-constant set in the EPR instrument. We used two different time constants, τ_1 = 81.9 and τ_2 = 2.6 ms. The latter value is the lowest time resolution attainable by our EPR instrumentation.

Data collection was controlled by a personal computer. LabView software was used to control magnetic field B, settings of the digital oscilloscope, and data acquisition. Typically, 100 transient signals were averaged from on-resonance conditions and subtracted from those recorded under off-resonance conditions to eliminate the background signal induced by the shuttered light. First-derivative 2D EPR spectra were obtained as a function of both time and magnetic field. Four-hundred points of transient signal were recorded at 128 different field values. The 400 × 128 matrix generated a 2D time-field data set that allowed for the acquisition of the time evolution of transient EPR-spectra.

2-2. Reagents. Oxygen was purchased from Matheson (research grade). The Sens species employed were $C_{10}H_8$, perdeuterated naphthalene ($C_{10}D_8$), and perfluoronaphthalene ($C_{10}F_8$), all purchased from Aldrich. All reagents were used as received. The majority of the experiments reported here were performed with $C_{10}H_8$.

3. RESULTS AND DISCUSSION

3-1. EPR of $O_2(^1\Delta_g)$ Generated in Steady-State Irradiation of Naphthalene in a Sealed Cell. $O_2(^1\Delta_g)$ was produced according to reaction 1, which is a triplet−triplet annihilation that occurs with a probability lower than the spin-statistical factor of $^1/_9$ under the collision of two triplet molecules.[6]

A series of experiments were performed in sealed EPR cells containing O_2 at different P_{O_2} values and $C_{10}H_8$ vapor (cf. section 2-1). In these experiments, we used O_2 with P_{O_2} = 0.10−0.50 Torr, leading to a total gas pressure estimation (including $C_{10}H_8$) of 0.18−0.58 Torr. Spectra recorded at the total gas pressure of 0.28 Torr, T = 293 K are shown in Figure 3. In the dark, a sharp and strong $O_2(^3\Sigma_g^-)$ component at B = 10 544.68 G (g = 0.6522) was readily observed (Figure 3a). Upon photoexcitation, the intensity of the component of the $O_2(^3\Sigma_g^-)$ spectrum noticeably decreases, and the spectrum of $O_2(^1\Delta_g)$ is observed (Figure 3b).[8−14] The nearly symmetrical quartet of lines at low field is observed at the exact position reported for $O_2(^1\Delta_g)$.[4−8] The EPR spectrum of $O_2(^1\Delta_g)$ disappears in the dark after the termination of the photoexcitation. No $O_2(^1\Delta_g)$ signal was detected under photoexcitation in the absence of $C_{10}H_8$ vapor. The measured and calculated g factors of the four lines are presented in Table 1.

Table 1. Observed and Calculated g Factor Values for Components of the $O_2(^1\Delta_g)$ EPR Spectrum

transition M_J[4,8]	B (G)[a]	observed g[a]	calculated g[b]
−2 → −1	10 486.00	0.655	0.65598
−1 → 0	10 375.68	0.662	0.66265
0 → +1	10 264.67	0.669	0.66955
+1 → +2	10 151.75	0.677	0.67668

[a]Obtained from the spectrum presented in Figure 3b. Microwave frequency ν = 9.62492 GHz. [b]Data from ref 8 (g) were calculated by accounting for higher-order-energy terms and the rotational constant of $O_2(^1\Delta_g)$.[8]

Table 1 demonstrates good agreement between the experimental and calculated g-factor values and confirms the correct assignment of the $O_2(^1\Delta_g)$ spectrum.[4,8] As expected, g is close to $^2/_3$.[8,14]

The relative intensity of each of the four components of the spectrum of $O_2(^1\Delta_g)$ is of interest. For a given transition $|i\rangle \rightarrow |f\rangle$, the intensity of the corresponding line is determined by the product of the transition probability W_{if} and the difference in the population Δp_{if} between the states $|i\rangle$ and $|f\rangle$. In the case of $O_2(^1\Delta_g)$, by considering the right quantum numbers in the ensemble (J = 2, M_J = −2, −1, 0, +1, +2) for the different EPR transitions (S = 0, J = Λ = 2, ΔM_J = ±1), and the operator J_y, Fermi−Wentzel's golden rule[9] can be used to calculate W_{if}. The calculation results in a probability ratio of $2:6^{1/2}:6^{1/2}:2$ for the four considered lines. This calculated probability ratio is very similar to the ratio of observed intensities in the spectra (Table 2).

dx.doi.org/10.1021/jp403648d | J. Phys. Chem. A 2013, 117, 5232−5240

Table 2. Observed and Calculated Relative Intensities of the Four Transitions in the EPR Spectrum of $O_2(^1\Delta_g)$

transition $\|M_J\rangle \rightarrow \|M_{J+1}\rangle$	$\|+2\rangle \rightarrow \|+1\rangle$	$\|+1\rangle \rightarrow \|0\rangle$	$\|0\rangle \rightarrow \|-1\rangle$	$\|-1\rangle \rightarrow \|-2\rangle$
observed intensity[a]	2.00 ± 0.00	2.78 ± 0.05	2.64 ± 0.15	1.77 ± 0.31
calculated intensity[b]	2.00	~2.45	~2.45	2.00

[a]Observed values are normalized to 2.00 in this transition. [b]According to Fermi–Wentzel's golden rule.[18]

The data presented in Table 2 demonstrates small differences in the values of Δp_{if} for the four components of $O_2(^1\Delta_g)$ under consideration. A noticeable deviation of one or more components from their expected intensities could be ascribed to a non-Boltzmann population of their corresponding spin-rotational states or to spin polarization. The observed lack of spin polarization in the 10–100 ms time span is expected because of the efficient spin-rotational relaxation of $O_2(^1\Delta_g)$.

$O_2(^1\Delta_g)$ is generally produced in the presence of a large excess of ground-state $O_2(^3\Sigma_g^-)$. Thus, the simultaneous appearance of the components of the EPR spectrum of the ground-state $O_2(^3\Sigma_g^-)$ can be used as a convenient internal standard for measuring $O_2(^1\Delta_g)$ concentration.[13,14]

$C_{10}H_8$ was the preferred Sens (section 2-2) because of its high vapor pressure of $P_{C_{10}H_8}$ = 0.05 Torr at 290 K.[19] However, under prolonged irradiation of $C_{10}H_8$ in the sealed cell, we observed that EPR signals for both $O_2(^1\Delta_g)$ and $O_2(^3\Sigma_g^-)$ completely disappeared after 18 min under our conditions (T = 293 K, P_{O_2} = 0.25 Torr).

Identification of the products of the photochemistry reaction(s) of $C_{10}H_8$ and other Sens was not the main focus of this or previous studies. The formation of endoperoxides is expected in a reaction of $C_{10}H_8$ with $O_2(^1\Delta_g)$ (cf. section 3-5, reaction 6).[6,15a] Oxidation of $^3C_{10}H_8$* by $O_2(^3\Sigma_g)$ can also take place (cf. section 3-5, reaction 9). It is also reasonable to expect that $C_{10}F_8$ is more stable during photoexcitation in an O_2 atmosphere than in $C_{10}H_8$.[13] At the same time, we observed the disappearance of all EPR signals in the case of $C_{10}F_8$ within 21 min under experimental conditions similar to those used in ref 13. Thus, under our experimental conditions, $C_{10}F_8$ is only slightly more stable than $C_{10}H_8$. A gradual decay of EPR signals under irradiation makes it difficult to prolong scanning with the goal of increasing the signal-to-noise ratio, S/N. As a result, we used the shortest possible acquisition time of 167 s, conducted one scan, and used a sealed sample only once.

We were interested in estimating the yields Φ of $O_2(^1\Delta_g)$ formation with the three Sens. For that purpose, we compared the relative concentrations of $O_2(^3\Sigma_g^-)$ as a ratio of double integrals of a selected component in the EPR spectrum of $O_2(^3\Sigma_g^-)$ (Figure 2).[13] It is assumed that $O_2(^1\Delta_g)$ appears at the expense of a decrease in $O_2(^3\Sigma_g^-)$ concentration. We define $[O_2(^3\Sigma_g^-)_{light}]$ and $[O_2(^3\Sigma_g^-)_{dark}]$ as the concentration of $O_2(^3\Sigma_g^-)$ during irradiation and in the dark, respectively. Thus, Φ is defined by eq 2:

$$\Phi = 1 - \frac{[O_2(^3\Sigma_g^-)_{light}]}{[O_2(^3\Sigma_g^-)_{dark}]} = 1 - \frac{k' \iint_{\text{selected line}} S_{light}(^3\Sigma_g^-)\ \text{dB dB}}{k'' \iint_{\text{selected line}} S_{dark}(^3\Sigma_g^-)\ \text{dB dB}} \quad (2)$$

The proportionality coefficients k' and k'' are unknown. Here, S_{Dark} and S_{Light} are the signals of the selected $O_2(^3\Sigma_g^-)$ component in the dark and under irradiation, respectively. The unknown constants k' and k'' depend on both the fraction of the area under the selected individual component and the total area calculated for the EPR spectrum of $O_2(^3\Sigma_g^-)$, assuming the same experimental conditions. Control experiments demonstrate that the irradiation of pure O_2 does not affect the intensity of the observed $O_2(^3\Sigma_g^-)$ component in the EPR spectra (although it is theoretically possible that irradiation could heat the gas inside the cell and affect the $O_2(^3\Sigma_g^-)$ component). Thus, we assume that $k' = k''$. In our experiments, P_{O_2} = 0.25 Torr and T = 293 K. Yields Φ (eq 2) of $O_2(^1\Delta_g)$ obtained under such assumptions are presented in Table 3.

Table 3. Yields (Φ) of the Generation of $O_2(^1\Delta_g)$ in Different Experiments in Sealed Cells[a]

experiment	$C_{10}H_8$ sensitization[b]	$C_{10}D_8$ sensitization[b]	$C_{10}F_8$ sensitization[b]
Φ	0.26	0.28	0.25
experiment	microwave discharge, O_2 flow conditions	$C_{10}H_8$ sensitization, O_2 flow conditions[b]	$C_{10}H_8$ sensitization, O_2 flow conditions[c]
Φ	>0.16	0.29	0.19

[a]Experiments at 293 K and P_{O_2} = 0.25 Torr. [b]Excitation was through a water filter and collimated lenses. [c]Excitation was through a water filter, collimated lenses, and a quartz rod (cf. Figure 1).

It is difficult to obtain the determination error of Φ. The decay of $O_2(^3\Sigma_g^-)$ in irreversible photochemical reactions (cf. above) and the presented Φ values in the sealed cells are probably the upper limits of the real Φ. However, the Φ values presented in Table 3 can be reliably used for comparison to each other.

3-2. EPR of $O_2(^1\Delta_g)$ Generated under Steady-State Irradiation of $C_{10}H_8$ and by Microwave Discharge within Oxygen Flow. The observed EPR spectra of $O_2(^1\Delta_g)$ generated by photosensitization with $C_{10}H_8$ and by microwave discharge in O_2 flow are presented in Figure 4.

In comparable experiments, microwave discharge typically leads to a higher concentration of $O_2(^1\Delta_g)$ and therefore to more intensive EPR signals than that for $O_2(^1\Delta_g)$ obtained by reaction 1.[8,12−14] The Φ values measured in the two cases (microwave discharge and photosensitization experiments) are presented in Table 3. One can compare Φ values (0.26, 0.28, and 0.25) among the photosensitization experiments carried out in the stationary setup. EPR signals of $O_2(^1\Delta_g)$ generated by microwave discharge are slightly weaker in intensity than EPR signals obtained by photosensitization under very similar conditions (cf. Figure 4). We note that in previous experiments, microwave discharge was reported to cause much higher intensity signals.[4,7] In addition, Φ values obtained in flow systems are close to those obtained in sealed cells. This means that the irreversible disappearance of O_2 resulting from photochemical reactions in the sealed cells was low under the conditions of a single scan.

In our work, we observed that P_{O_2} and T strongly affect the yield and kinetics of $O_2(^1\Delta_g)$ decay. Figure 5 displays the EPR spectra of $O_2(^1\Delta_g)$ recorded at two different temperatures. Our

dx.doi.org/10.1021/jp403648d | J. Phys. Chem. A 2013, 117, 5232−5240

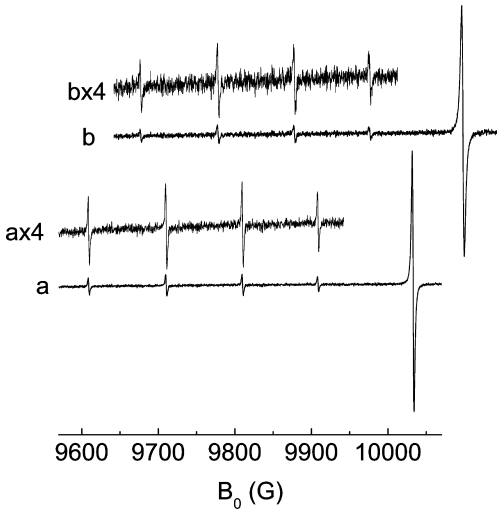

Figure 4. EPR spectra of $O_2(^1\Delta_g)$ generated by microwave discharge (a) and by photosensitization with $C_{10}H_8$ in the O_2 flow (b). P_{O_2} = 0.2 Torr and T = 293 K (cf. Experimental Section 2-1).

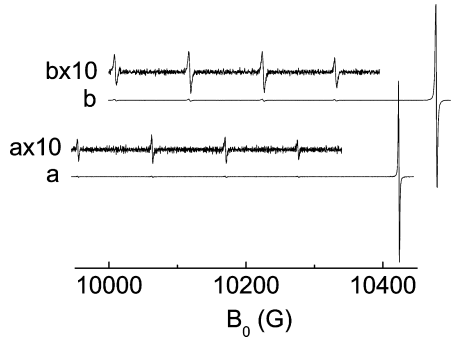

Figure 5. EPR spectra of $O_2(^1\Delta_g)$ generated by photosensitization experiments in the O_2 flow with $C_{10}H_8$ at 298 K (a) and T = 313 K (b). Spectra (a) and (b) were obtained at P_{O_2} = 0.2 Torr. Four scans were performed for each spectrum.

evaluations of Φ at different T and the same P_{O_2} are shown in Figure 6.

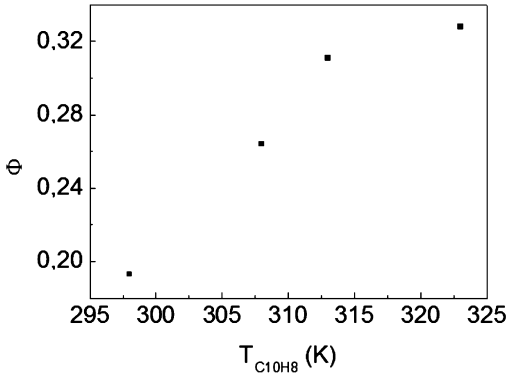

Figure 6. Photosensitization efficiency Φ as a function of T at P_{O_2} = 0.2 Torr in the O_2 flow system.

Figure 6 demonstrates that Φ increases with an increase in T. Evidently, increasing T leads to an increase in the pressure (concentration) of $C_{10}H_8$ inside the cell in the cavity, which in turn leads to a higher frequency of collisions between $C_{10}H_8$ and $O_2(^3\Sigma_g^-)$ and a higher yield of $O_2(^1\Delta_g)$ within the studied limits. Is it well known that only higher T itself leads to a higher frequency of gas-phase collisions.

3-3. EPR Line Widths of $O_2(^3\Sigma_g^-)$ and $O_2(^1\Delta_g)$. The line width of individual components in EPR spectra is determined by the rate of paramagnetic relaxation: the faster the relaxation, the broader the line width. Figure 2 demonstrates that the experimental line width of an $O_2(^3\Sigma_g^-)$ component increases with an increase in P_{O_2}. The examination of $O_2(^3\Sigma_g^-)$ line widths led to the conclusion that line widths of both $O_2(^1\Delta_g)$ and $O_2(^3\Sigma_g^-)$ are narrower under conditions of microwave discharge compared to conditions of sensitization by $C_{10}H_8$ (the two experiments were conducted under similar conditions with respect to P_{O_2} and T, cf. Figure 4).

Spin relaxation in the gas phase is expected to take place mainly by spin-rotational interactions. The collisions of O_2 with other molecules affect molecular rotation of O_2 and also modulate electronic-dipolar spin-spin interactions. Both factors lead to an increase in paramagnetic relaxation and line broadening.

We found that the line width of $O_2(^3\Sigma_g^-)$ is linearly dependant on P_{O_2} (cf. Appendix Table A). Similar measurements of EPR line widths of $O_2(^3\Sigma_g^-)$ as function of P_{O_2} at lower pressures of 0.04−0.5 Torr have been previously reported and show a similar linear dependence between the line-width $O_2(^3\Sigma_g^-)$ component and P_{O_2}.[20]

Table B (Appendix) presents the measurements of EPR intensity of $O_2(^1\Delta_g)$ and $O_2(^3\Sigma_g^-)$ components at different temperatures. It follows from Table B that the yield of $O_2(^1\Delta_g)$ formation increases with an increase in T. The probable reason for this result is the acceleration of reaction 1 by increasing T.

Despite a modest S/N ratio in the EPR measurements of the $O_2(^1\Delta_g)$ signals, we observed a linear dependence between the line widths of $O_2(^1\Delta_g)$ and P_{O_2}, as shown in Figure 7.

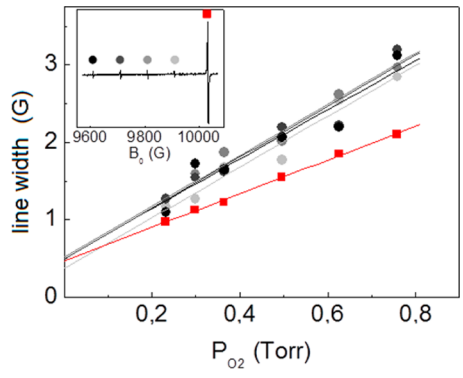

Figure 7. Line widths of EPR spectra of both $O_2(^3\Sigma_g^-)$ (red filled boxes) and $O_2(^1\Delta_g)$ (light-gray filled circles, medium-gray filled cirles, dark-gray filled circles, and black filled circles) as a function of P_{O_2} in O_2 flow under irradiation of $C_{10}H_8$ at 318 K (cf. Figure 2 for comparison to line widths of $O_2(^3\Sigma_g^-)$ signals recorded in the absence of light irradiation).

It follows from Figure 7 that all four lines of $O_2(^1\Delta_g)$ are similarly sized and within the experimental error, which was expected. To the best of our knowledge, this is the first experimental study of the EPR line widths of $O_2(^1\Delta_g)$ in the gas phase at different P_{O_2} values.

dx.doi.org/10.1021/jp403648d | J. Phys. Chem. A 2013, 117, 5232−5240

One would expect that line widths of $^1O_2$ and $^3O_2$ are similar because these molecules are of similar size and have similar rotational-correlation times and frequency of collisions under the same T and P. However, we have noticed slightly different dependencies of the line widths of $^1O_2$ and $^3O_2$ on P_{O_2} (cf. Figure 7). This difference is a reflection of the fact that the line widths of $^1O_2$ and $^3O_2$ are close to each other but not equal.

We observed that the line width of $O_2(^3\Sigma_g^-)$ increases as P_{O_2} increases (Figure 2). It increases at a constant P_{O_2} in the presence of $C_{10}H_8$ in the dark as well. We conclude that collisions between $O_2(^3\Sigma_g^-)$ and $O_2(^3\Sigma_g^-)$ and collisions between $O_2(^3\Sigma_g^-)$ and $C_{10}H_8$ accelerate the paramagnetic relaxation of $O_2(^3\Sigma_g^-)$. During photoexcitation of $C_{10}H_8$, the line width of $O_2(^3\Sigma_g^-)$ decreased, apparently resulting from a noticeable (~20%) decrease in the $O_2(^3\Sigma_g^-)$ concentration. As expected, the line width of $O_2(^3\Sigma_g^-)$ increases as P_{O_2} increases under irradiation as well as in the dark.

3-4. TR EPR of $O_2(^1\Delta_g)$ Generated by Photosensitization with $C_{10}H_8$ in the O_2 Flow. The TR EPR 2D spectrum of the third component (g = 0.669, Table 1) of $O_2(^1\Delta_g)$ in the time range of a few seconds is shown in Figure 8.

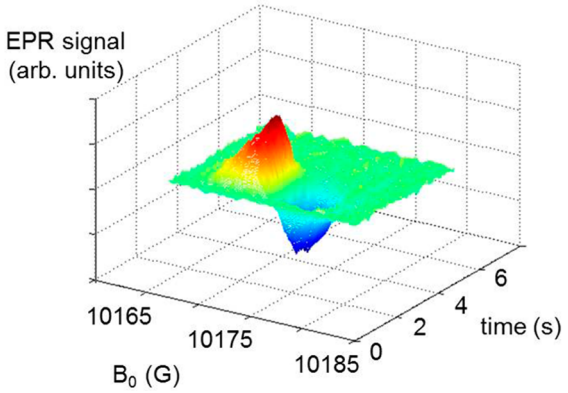

Figure 8. TR EPR 2D spectrum of the third component of $O_2(^1\Delta_g)$ generated by photosensitization with $C_{10}H_8$ in the O_2 flow, P_{O_2} = 0.44 Torr and T = 318 K. The experimental parameters were EPR time constant τ = 81.92 ms, microwave attenuation 10 dB, 40 accumulations for each B value, irradiation period of 1.5 s, and dark period of 3.5 s.

The details of these TR EPR 2D measurements are presented in section 2-1.

The transient EPR signals of the four $O_2(^1\Delta_g)$ lines were recorded with the magnetic field set on B^+_{max} spectral positions, corresponding to the maxima of the four first-derivative lines. These four maxima are denoted as a^+, b^+, c^+, and d^+ and are presented in Figure 9.

It has been reported[8a] that the decay kinetics of $O_2(^1\Delta_g)$ do not follow a first-order law. We used a biexponential law (eq 3) to describe the kinetics of $O_2(^1\Delta_g)$ decay (red traces in Figure 9):

$$I_{obs} = I_1 \exp(-t/t_1) + I_2 \exp(-t/t_2) \quad (3)$$

In eq 3, I_{obs} is the observed EPR signal intensity and I_1, I_2, t_1, and t_2 are fitting parameters. The instant at which the signal begins to disappear was selected as t = 0 in the fitting process. In this report, we used arbitrary units on the same scale to obtain I_1 and I_2 .

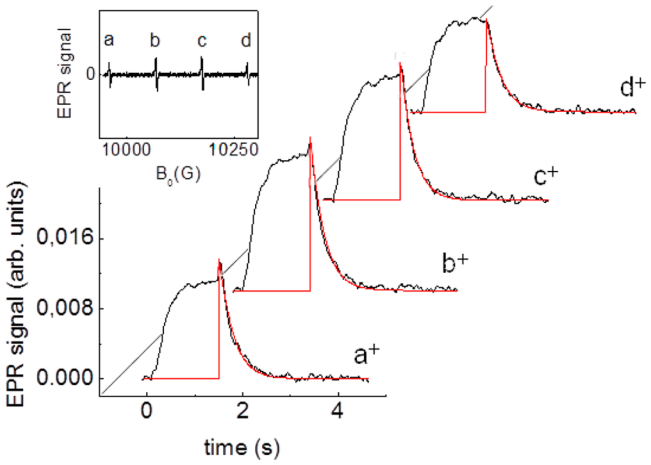

Figure 9. Time evolution of a^+, b^+, c^+, and d^+ maxima in the EPR spectrum of $O_2(^1\Delta_g)$. The transient signals were observed at P_{O_2}= 0.44 Torr and T = 318 K. With the exception of 100 accumulations, the instrument parameters are identical to those described in the caption of Figure 8. The calculated curves (red traces) are the simulations of decay kinetics using eq 3.

Similar transient signals were recorded at field B^-_{max} (a^-, b^-, c^-, and d^-), corresponding to the minima of the four first derivatives of the EPR spectrum (results not shown). They demonstrated the same kinetics of decay as their corresponding positive counterparts.

We noticed that the fast component of I_{obs} decay has t_1 close to 82 ms and that t_1 does not depend on the selected component or experimental conditions. This time, t_1, is in fact the shortest possible time constant, τ = 82 ms, that was set up for the spectrometer (cf. section 2-1). Therefore, we modified the simulations by setting I_1 and t_1 for all simulations equal to 2.0 arb units and 82 ms, respectively. I_1 and t_1 are instrument parameters, and we do not use them in our kinetic analysis. Values of t_2 are much longer than the t_1 of the instrument and can be identified as the lifetime τ of $O_2(^1\Delta_g)$.

Table 4 presents the best values of I_2 and t_2 as the average values from multiple experiments.

Table 4. Fitting Parameters I_2 and t_2 of Equation 3 Used in Simulation of Kinetics of the Decay of a^+, b^+, c^+, and d^+ Signals in the EPR Spectrum of $O_2(^1\Delta_g)$

	I_2 (arb units)[a]	t_2 (ms)
a^+	15.8 ± 1.9	270 ± 45
b^+	19.6 ± 2.7	275 ± 55
c^+	18.3 ± 2.5	255 ± 50
d^+	12.7 ± 1.8	280 ± 55

[a]We used arbitrary, same-scale units for reporting I_1 and I_2 values, as described in the text.

It is obvious that I_2 values for the two central lines b^+ and c^+ in the EPR spectrum of $O_2(^1\Delta_g)$ are larger than the corresponding values for lines a^+ and d^+ (Table 4) because the central components in the spectrum are more intense (cf. Figures 3–5, 9). The measured t_2 values are equivalent and within the experimental error (Table 4), supporting the expectation that we are monitoring the disappearance of the same species.

In agreement with reported observations,[14] the kinetics experiments described below demonstrate that the appearance

dx.doi.org/10.1021/jp403648d | J. Phys. Chem. A 2013, 117, 5232–5240

of the $O_2(^1\Delta_g)$ EPR signal occurs with the concomitant disappearance of the $O_2(^3\Sigma_g^-)$ EPR signal. Pertinent data are presented in the Figure 10 where a comparison between the time evolutions of the positive first derivative part of $O_2(^1\Delta_g)$ (gray and black traces) and $O_2(^3\Sigma_g)$ (red trace) signals is shown.

The transient $O_2(^3\Sigma_g^-)$ signal has been reduced by a factor of −13.7 for clarity (Figure 10). The observed spikes in the curves

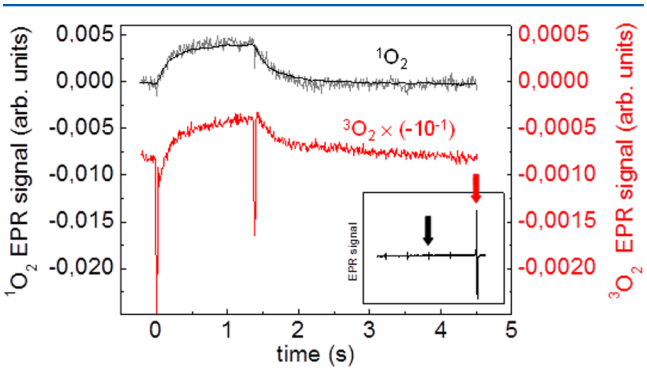

Figure 10. Time evolution of the positive portions of $O_2(^1\Delta_g)$ components observed with time constants of τ = 2.56 ms (gray trace) and τ = 81.92 ms (black trace) and the positive portion of $O_2(^3\Sigma_g^-)$ with τ = 2.56 ms (red trace). The transient signals were recorded at P_{O_2} = 0.40 Torr and T = 298 K in a sealed cell.

are attributed to the instantaneous loss of frequency lock between the EPR detector and gun diode (AFC control) at the moment of shutter action.

The good overlap of the observed kinetics recorded with τ = 2.56 ms (gray trace) and τ = 81.92 ms (black trace) in Figure 10 demonstrates that τ = 81.92 ms is a sufficiently short time to measure the kinetics of $O_2(^1\Delta_g)$ and $O_2(^3\Sigma_g^-)$ evolution. It then follows from Figure 10 that the $O_2(^3\Sigma_g^-)$ signal does not reach a plateau at the end of the observation. This fact can be attributed to the contribution of the irreversible decay of $O_2(^3\Sigma_g^-)$ in the sealed cells (cf. section 3-1).

3-5. Decay of EPR Signals of $O_2(^1\Delta_g)$ Generated by Photosensitization with $C_{10}H_8$ within O_2 Flow. To obtain information on the possible reactions of $O_2(^1\Delta_g)$, we obtained multiple TR EPR scans of an $O_2(^1\Delta_g)$ component at different P_{O_2} and $T_{C_{10}H_8}$ within O_2 flow. Decay kinetics were simulated with eq 3, and I_1 and t_1 were set to the same values as described in section 3-4. Figure 11 shows the transient signals of $O_2(^1\Delta_g)$ recorded at different P_{O_2} and the same T.

Table 5 summarizes the values of I_2 and t_2 obtained at different P_{O_2} and two different T.

On the basis of the results in Table 5, we can infer that the signal of the largest intensity (I_2) is observed at a medium value of P_{O_2}. Apparently the increased frequency of collisions at higher P_{O_2} leads to a higher $O_2(^1\Delta_g)$ concentration (cf. section 3-1), but a further increase in P_{O_2} leads to $O_2(^1\Delta_g)$ quenching in collisions with $O_2(^3\Sigma_g^-)$. Thus, there is an optimal medium pressure (Table 5) for the observation of the most intense signals, which is P_{O_2} = 0.4 Torr, and T = 293 K.

The same considerations are applicable to t_2, Table 5. The plot in Figure 12 shows the dependence of t_2 on P_{O_2} with a maximum.

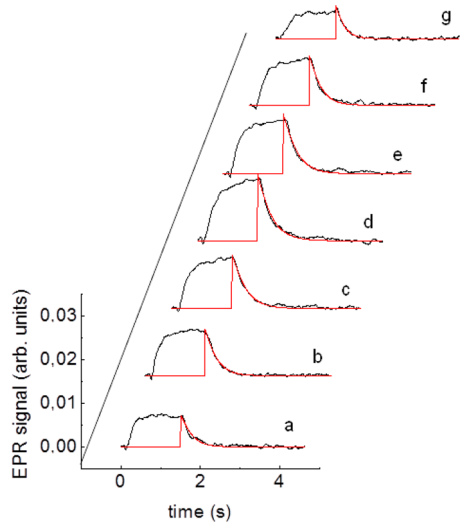

Figure 11. Observed time evolution of the positive portion of the third $O_2(^1\Delta_g)$ line c^+ at 293 K and varied P_{O_2} (mTorr): (a)174, (b) 231, (c) 298, (d) 364, (e) 431, (f) 496, and (e) 625. Except for the accumulation number (in this case 100), the instrument parameters are identical to those described in the caption of Figure 8. Black curves are the experimental traces, and red traces are the data fitted to eq 3.

Table 5. Fitting Parameters Used in Equation 3 Describing the Decay of the Third Component c^+ in the EPR Spectrum of $O_2(^1\Delta_g)$ under Different Experimental Conditions[a]

P_{O_2} (mTorr)	T (K)	I_2 (arb units)	t_2 (ms)
175	293	9.3 ± 1.3	320 ± 65
	308	9.7 ± 1.3	240 ± 45
231	293	15.8 ± 1.9	355 ± 60
	308	13.4 ± 1.8	255 ± 50
298	293	17.8 ± 2.4	405 ± 80
	308	14.9 ± 1.7	315 ± 50
364	293	14.4 ± 1.9	390 ± 70
	308	15.9 ± 2.1	320 ± 60
431	293	15.5 ± 2.2	355 ± 70
	308	15.4 ± 1.9	300 ± 50
496	293	12.0 ± 1.6	295 ± 55
	308	13.4 ± 1.8	255 ± 50
625	293	12.5 ± 1.9	240 ± 50
	308	9.8 ± 1.3	190 ± 35

[a]Compare Figure 9. See the text for details.

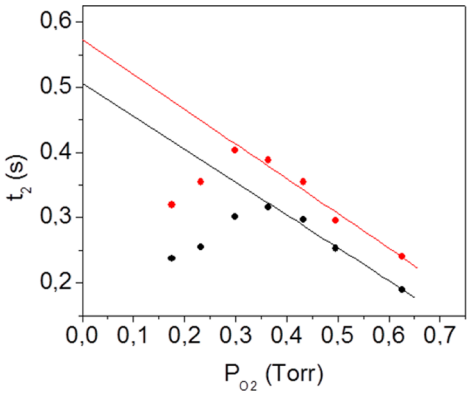

Figure 12. Dependence of t_2 (Table 5) on P_{O_2} obtained at 293 K (black filled circles) and 308 K (red filled circles), cf. the text.

dx.doi.org/10.1021/jp403648d | J. Phys. Chem. A 2013, 117, 5232−5240

We estimated t_2 at $P_{O_2} = 0$ to be $t_2 = 570 \pm 25$ and $t_2 = 510 \pm 25$ ms at 293 and 308 K, respectively, by extrapolating the linear fit of several points to $P_{O_2} = 0$ (Figure 12). This value corresponds to the lifetime of $O_2(^1\Delta_g)$ in the limiting case of an absence of $O_2(^3\Sigma_g^-)$ molecules. $O_2(^1\Delta_g)$ decays by reactions (cf. below) and by collisions with $O_2(^3\Sigma_g^-)$ molecules.

Reactions 4−8 are expected to contribute to $O_2(^1\Delta_g)$ decay:

$$O_2(^1\Delta_g) + O_2(^3\Sigma_g^-) \rightarrow 2O_2(^3\Sigma_g^-) \quad (4)$$

$$O_2(^1\Delta_g) + O_2(^1\Delta_g) \rightarrow O_2(^3\Sigma_g^-) + O_2(^1\Sigma_g^+) \quad (5)$$

$$O_2(^1\Delta_g) + C_{10}H_8 \rightarrow \text{possibly endoperoxide} \quad (6)$$

$$O_2(^1\Delta_g) + {}^3C_{10}H_8{}^* \rightarrow O_2(^3\Sigma_g^-) + C_{10}H_8 \quad (7)$$

$$O_2(^1\Delta_g) + \text{wall} \rightarrow O_2(^3\Sigma_g^-) \quad (8)$$

Reaction 8 takes into consideration the deactivation of $O_2(^1\Delta_g)$ on the walls of the flow quartz tube. Unfortunately, not all rate constants of the reactions are known, prohibiting a strict kinetic analysis of $O_2(^1\Delta_g)$ decay. The kinetics of $O_2(^1\Delta_g)$ decay is neither first- nor second-order; instead, it fits nicely to the biexponential law (eq 3, cf. section 3-4).

The decay of $O_2(^1\Delta_g)$ by luminescence is very slow in the gas phase where the radiation lifetime of $O_2(^1\Delta_g)$ has been previously reported to be ∼45 min.[21] Thus, radiative processes may be excluded from the analysis.

We confirmed in the direct TR EPR experiments that the appearance of $O_2(^1\Delta_g)$ occurs at the same rate as the disappearance of $O_2(^3\Sigma_g^-)$ under the photoexcitation of Sens. Therefore, other possible reactions of $O_2(^3\Sigma_g^-)$ decay proceed much slower than reaction 1. The most probable alternative path for $O_2(^3\Sigma_g^-)$ decay could be reaction 9:

$$^3\text{Sens}^* + O_2(^3\Delta_g^-) \rightarrow \text{chemical product(s)} \quad (9)$$

We now compare our results to the results of ref 14. Yagi et al.[14] studied the formation and decay of $O_2(^1\Delta_g)$ with $C_{10}F_8$ as a sensitizer at room temperature. The diameter of the cell used in ref 14 was similar to that used in our study, and P_{O_2} was varied in the range of 0.2−1.0 Torr.[14] The lifetime $\tau = 7$ s of $O_2(^1\Delta_g)$ was observed at $P_{O_2} = 0.6$ Torr.[14] Our kinetic curves (Figures 8−11) demonstrate a lack of $O_2(^1\Delta_g)$ EPR signal after several milliseconds. Therefore, the results of ref 14 are in disagreement with the results that we obtained. Our measured τ values were in the range of 0.2−0.4 s (Figure 12). Moreover, ref 14 reports a linear increase in $O_2(^1\Delta_g)$ concentration with P_{O_2} increases of up to 1.0 Torr, whereas we observed a maximum for a similar dependence at $P = 0.4$ Torr (cf. the values of I_2 at different P_{O_2} in Table 5.)

The reason for the differences between our results and the results in ref 14 is not obvious. It is likely that in our case a more efficient quenching (eqs 4 and 5) takes place. A TR EPR study of $O_2(^1\Delta_g)$ with $C_{10}F_8$ used in ref 14 is currently underway.

4. CONCLUSIONS

Irradiation of triplet sensitizers under low $O_2(^3\Sigma_g^-)$ pressure leads to the formation of $O_2(^1\Delta_g)$, which is detectable by EPR spectroscopy. An interesting hypothesis suggests that the primary product of reaction 1 in the liquid phase is $O_2(^1\Sigma_g^+)$, which quickly decays with the formation of $O_2(^1\Delta_g)$.[7a,b] Our experiments do not allow for a confirmation or rejection of this hypothesis.

A significant fraction of $O_2(^3\Sigma_g^-)$, up to 30%, can be transformed to $O_2(^1\Delta_g)$ (cf. section 3-1 and ref 13). As a result, the presence of $O_2(^1\Delta_g)$ cannot be ignored in the analysis of the chemical composition of a polluted atmosphere.

The decay of transient signals of $O_2(^1\Delta_g)$ is accompanied by the almost complete regeneration of $O_2(^3\Sigma_g^-)$. We use the term almost because sensitizers $C_{10}H_8$ and $C_{10}F_8$ participate in a slow, irreversible photochemical reaction with $O_2(^3\Sigma_g^-)$ and possibly $O_2(^1\Delta_g)$. The lifetime τ of $O_2(^1\Delta_g)$ in our experiments with $C_{10}H_8$ was found to be $\tau < 1$ s at pressures of 0.17−0.63 Torr and $T = 293$−323 K. At a medium pressure of $P_{O_2} = 0.4$ Torr, we observed the largest EPR signal and the longest lifetime of $O_2(^1\Delta_g)$ $\tau = 0.4$ s ($T = 293$ K). These values are much shorter than the $\tau = 7$ s reported in ref 14 and were obtained under similar experimental conditions with Sens $C_{10}F_8$. The reasons for such a discrepancy between the two studies are tentatively ascribed to higher rates of quenching of $O_2(^1\Delta_g)$ by $O_2(^3\Sigma_g^-)$ and Sens in the present work.

The extrapolation of dependencies at $P_{O_2} = 0$ enabled us to calculate the lifetime of $O_2(^1\Delta_g)$ to be $\tau = 575$ and 510 ms at 293 and 308 K, respectively. The kinetics of the components of the EPR decay spectrum fit a biexponential law (eq 3) in which the first exponent accounts for an instrument parameter. Parameter $t_2 \approx 100$−400 ms of the second exponent in eq 3 (Tables 4 and 5) was considered to have a lifetime τ of $O_2(^1\Delta_g)$ that decays by a pseudo-first-order law.

In this Article, we present the TR EPR 2D spectrum of one component of $O_2(^1\Delta_g)$ produced by photosensitization with $C_{10}H_8$ in a flow system and clearly demonstrate the time evolution of $O_2(^1\Delta_g)$. We found that line widths of $O_2(^1\Delta_g)$ and $O_2(^3\Sigma_g^-)$ increase linearly but vary somewhat with an increase in P_{O_2}.

APPENDIX

Results presented in Table A evidence that the line width of $O_2(^3\Sigma_g^-)$ is linearly dependant on P_{O_2}.

Table B reports EPR intensities of $O_2(^1\Delta_g)$ and $O_2(^3\Sigma_g^-)$ components at different temperatures.

Table A. Linear Regression Parameters for Measured Line Widths of Four Components of the EPR Spectrum of $O_2(^1\Delta_g)$ and the Selected Component of $O_2(^3\Sigma_g^-)$ in Its EPR Spectrum vs P_{O_2}[a]

	$O_2(^1\Delta_g)$ line I	$O_2(^1\Delta_g)$ line II	$O_2(^1\Delta_g)$ line III	$O_2(^1\Delta_g)$ line IV	$O_2(^3\Sigma_g^-)$ selected line
A	362.72 ± 160.79	507.95 ± 161.77	488.57 ± 225.59	503.11 ± 260.54	465.17 ± 24.5
B	3.29 ± 3.23379 × 10^{-4}	3.30 ± 3.25351 × 10^{-4}	3.30 ± 4.53709 × 10^{-4}	3.20 ± 5.23998 × 10^{-4}	2.18 ± 4926.85 × 10^{-5}

[a]Regression was calculated by (line width) = $A + BP_{O_2}$. The linear fits are demonstrated in Figure 7.

dx.doi.org/10.1021/jp403648d | J. Phys. Chem. A 2013, 117, 5232−5240

Table B. Areas under Each Component of the $O_2(^1\Delta_g)$ EPR Spectrum and of the Selected Component of $O_2(^3\Sigma_g^-)$ During Irradiation of $C_{10}H_8$ at Different Temperatures[a]

T (K)	area singlet I	area singlet II	area singlet III	area singlet IV	area singlet sum (S)	area triplet (light)[b] (T)	S/T
298	0.17813	0.29820	0.32304	0.22752	1.02689	27.08401	0.0379
308	0.17121	0.37770	0.41973	0.28380	1.25244	24.70844	0.0507
313	0.27754	0.47099	0.61255	0.32994	1.69102	23.12982	0.0731
323	0.42857	0.54099	0.68440	0.37299	2.02695	22.56103	0.0898

[a]Calculated values. The arb area units are the same as those used in Table 4, P_{O_2} = 0.2 Torr. In the absence of irradiation, we obtained the same area at different T under the studied component of $O_2(^3\Sigma_g^-)$ (cf. Figure 5). [b]The area under the selected $O_2(^3\Sigma_g^-)$ component that was measured in the absence of $C_{10}H_8$ and light irradiation is 33.56146 ± 0.01.

AUTHOR INFORMATION

Corresponding Author

*E-mail: igor.khudyakov@solutia.com.

Present Address

[§]Solutia Inc., a subsidiary of Eastman, Fieldale, VA 24089

Notes

The authors declare no competing financial interest.

N. J. Turro passed away on 11/24/2012.

REFERENCES

(1) Following the general assumption, in this paper we name dioxygen O_2 as oxygen.

(2) Foote, C. S.; Clennan, E. L. Properties and Reactions of Singlet Dioxygen. In *Active Oxygen in Chemistry*; Foote, C. S., Valentine, J. S., Greenberg. A., Liebman, J. F., Eds.; Capman and Hall: London, 1995; pp 105−140.

(3) Greer, A. Christopher Foote's Discovery of the Role of Singlet Oxygen [$^1O_2(^1\Delta_g)$] in Photosensitized Oxidation Reactions. *Acc. Chem. Res.* **2006**, *39*, 797−804.

(4) Kearns, D. R. Physical and Chemical Properties of Singlet Molecular Oxygen. *Chem. Rev.* **1971**, *71*, 395−427.

(5) Schweitzer, C.; Schmidt, R. Physical Mechanisms of Generation and Deactivation of Singlet Oxygen. *Chem. Rev.* **2003**, *103*, 1685−1757.

(6) Turro, N. J.; Ramamurthy, V.; Scaiano, J. C. Molecular Oxygen and Organic Photochemistry. *Modern Molecular Photochemistry of Organic Molecules*; University Science Books: Sausalito, CA, 2010; Chapter 14.

(7) (a) Ogilby, P. R. Solvent Effects on the Radiative Transitions of Singlet Oxygen. *Acc. Chem. Res.* **1999**, *32*, 512−519. (b) Andersen, L. K.; Ogilby, P. R. Absorption Spectrum of Singlet Oxygen ($a^1\Delta_g \rightarrow b\ ^1\Sigma g^+$) in D_2O: Enabling the Test of a Model for the Effect of Solvent on Oxygen's Radiative Transitions. *J. Phys. Chem. A* **2002**, *106*, 11064−11069.

(8) Falick, A. M.; Mahan, B. H.; Myers, R. J. Paramagnetic Resonance Spectrum of the $^1\Delta_g$ Oxygen Molecule. *J. Chem. Phys.* **1965**, *42*, 1837−1838.

(9) Kearns, D. R.; Khan, A. U.; Duncan, C. K.; Maki, A. H. Detection of the Naphthalene-Photosensitized Generation of Single ($^1\Delta_g$) Oxygen by Paramagnetic Resonance Spectroscopy. *J. Am. Chem. Soc.* **1969**, *91*, 1039−1040.

(10) Wasserman, E.; Murray, R. W.; Kaplan, H. L.; Yager, Y. A. Electron Paramagnetic Resonance of $^1\Delta$ Oxygen from a Phosphite-Ozone Complex. *J. Am. Chem. Soc.* **1968**, *90*, 4160−4161.

(11) Wasserman, E.; Kuck, V. J.; Delavan, W. M.; Yager, W. A. Electron Paramagnetic Resonance of $^1\Delta$ Oxygen Produced by Gas-Phase Photosensitization with Naphthalene. *J. Am. Chem. Soc.* **1969**, *91*, 1040−1041.

(12) (a) Khudyakov, I. V.; Turro, N. J. Unpublished work, 1993. (b) Moscatelli, A. Ph.D. Thesis, Chemistry Department, Columbia University, New York, NY 2008.

(13) Yagi, M.; Takemoto, S.; Sasase, R. Measurement of Concentration of Singlet Molecular Oxygen in the Gas Phase by Electron Paramagnetic Resonance. *Chem. Lett.* **2004**, *33*, 152−153.

(14) Hasegawa, K.; Yamada, K.; Sasase, R.; Miyaazaki, R.; Kikuchi, A.; Yagi, M. Direct Measurements of Absolute Concentration and Lifetime of Singlet Oxygen in the Gas Phase by Electron Paramagnetic Resonance. *Chem. Phys. Lett.* **2008**, *457*, 312−314.

(15) (a) Pitts, J. N.; Khan, A. U.; Smith, E. B.; Wayne, R. P. Singlet Oxygen in the Environmental Sciences. Singlet Molecular Oxygen and Photochemical Air Pollution. *Environ. Sci. Technol.* **1969**, *3*, 241−247. (b) Fox, M. A.; Olive, S. Photooxidation of Anthracene on Atmospheric Particulate Matter. *Science* **1979**, *205*, 582−583.

(16) (a) Atkinson, R. Gas-Phase Tropospheric Chemistry of Organic Compounds: A Review. *Atmos. Environ.* **1990**, *24A*, 1−41. (b) Jones, I. T. N.; Bayes, K. D. Formation of $O_2(a\ ^1\Delta_g)$ by Electronic Energy Transfer in Mixtures of NO_2 and O_2. *J. Chem. Phys.* **1973**, *59*, 3119−3124.

(17) Wayne, C. E.; Wayne, R. P. *Photochemistry*; Oxford University Press: Oxford, U.K., 1999; p 70.

(18) Fermi, E. *Nuclear Physics*; University of Chicago Press: Chicago, 1950.

(19) Růžička, K.; Fulem, M.; Růžička, V. Recommended Vapor Pressure of Solid Naphthalene. *J. Chem. Eng. Data* **2005**, *50*, 1956−1970.

(20) Utter, R. G.; Gardiner, W. C. Conformation of Anomalous Pressure Dependence of Linewidths of the Electron Paramagnetic Resonance Spectrum of Molecular Oxygen. *J. Chem. Phys.* **1989**, *91*, 2054−2058.

(21) Bader, R. M.; Wright, A. C.; Whitlock, R. F. Absolute Intensities of the Discrete and Continuous Absorption Bands of Oxygen Gas at 1.26 and 1.065 μ and the Radiative Lifetime of the $^1\Delta_g$ State of Oxygen. *J. Chem. Phys.* **1965**, *43*, 4345−4350.